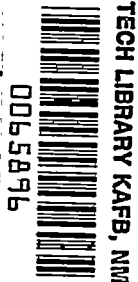


NACA TN 2876 L 026



TECH LIBRARY KAFB, NM

# NATIONAL ADVISORY COMMITTEE FOR AERONAUTICS

TECHNICAL NOTE 2876

THE PLANING CHARACTERISTICS OF TWO V-SHAPED  
PRISMATIC SURFACES HAVING ANGLES OF  
DEAD RISE OF  $20^{\circ}$  AND  $40^{\circ}$

By Derrill B. Chambliss and George M. Boyd, Jr.

Langley Aeronautical Laboratory  
Langley Field, Va.



Washington  
January 1953

AFL 2811  
TECHNICAL NOTE 2876  
AFL 2811

## TECHNICAL NOTE 2876

THE PLANING CHARACTERISTICS OF TWO V-SHAPED  
PRISMATIC SURFACES HAVING ANGLES OF  
DEAD RISE OF  $20^{\circ}$  AND  $40^{\circ}$ 

By Derrill B. Chambliss and George M. Boyd, Jr.

## SUMMARY

The principal planing characteristics have been obtained for two V-shaped prismatic surfaces having angles of dead rise of  $20^{\circ}$  and  $40^{\circ}$ . The load, wetted lengths, resistance, center-of-pressure location, and limited draft data are presented for speed coefficients up to 25.0, beam-loading coefficients from 0.85 to 87.33, keel-wetted-length-beam ratios up to approximately 8.0, and trims up to  $30^{\circ}$ . The data indicate that, for a given condition of load, speed, and trim, the wetted length, the distance of the center of pressure from the trailing edge, and the drag increase with an increase in the angle of dead rise.

## INTRODUCTION

A general program of research on the planing characteristics of a series of related prismatic surfaces has been undertaken by the National Advisory Committee for Aeronautics and is described in reference 1. The primary objective of this program is an extension of the range of experimental data on planing surfaces to cover the high trims and wetted lengths of interest in the design of high-speed water-based airplanes.

This paper presents the hydrodynamic force data for two V-shaped planing surfaces having angles of dead rise of  $20^{\circ}$  and  $40^{\circ}$ . Load, wetted lengths, resistance, center-of-pressure location, and limited draft data are given for speed coefficients up to 25.0, trims up to  $30^{\circ}$ , and wetted-length-beam ratios up to 8.0. Similar data for surfaces having angles of dead rise of  $20^{\circ}$  and  $40^{\circ}$  and horizontal chine flare are presented in references 1 and 2.

## SYMBOLS

b	beam of planing surface, ft
d	draft at trailing edge (measured vertically from undisturbed water level), ft
g	acceleration due to gravity, 32.2 ft/sec <sup>2</sup>
<i>l</i> <sub>c</sub>	chine wetted length, ft
<i>l</i> <sub>k</sub>	keel wetted length, ft
<i>l</i> <sub>m</sub>	mean wetted length, $\frac{l_c + l_k}{2}$ for these models, ft
<i>l</i> <sub>p</sub>	center-of-pressure location (measured along keel forward of trailing edge of planing surface), $\frac{M}{\Delta \cos \tau + R \sin \tau}$ , ft
M	trimming moment about trailing edge of planing surface at keel, ft-lb
Δ	vertical load, lb
F	friction, parallel to planing surface, lb
R	horizontal resistance, lb
R <sub>e</sub>	Reynolds number, $V_m l_m / \nu$
S	principal wetted area (bounded by trailing edge, chines, and heavy spray line) projected on plane parallel to keel, $l_m b$ , sq ft
S <sub>f</sub>	actual wetted area aft of stagnation line, sq ft
V	horizontal velocity, ft/sec
V <sub>m</sub>	mean velocity over planing surface, $\sqrt{V^2 \left(1 - \frac{C_{Lb}}{\cos \tau \frac{l_m}{b}}\right)}$
w	specific weight of water, lb/ft <sup>3</sup>
C <sub>Δ</sub>	load coefficient, $\Delta / wb^3$

$C_R$	resistance coefficient, $R/wb^3$
$C_V$	speed coefficient or Froude number, $V/\sqrt{gb}$
$C_f$	skin-friction coefficient, $\frac{F}{2 \rho S_f V_m^2} = \frac{\cos \beta \cos^2 \tau}{l_m \cos \tau - C_{Lb}} (C_{D_b} - C_{Lb} \tan \tau)$
$C_{Lb}$	lift coefficient based on beam, $\frac{\Delta}{\rho V^2 b^2} = 2 \frac{C_L}{C_V^2}$
$C_{D_b}$	drag coefficient based on beam, $\frac{R}{\rho V^2 b^2} = 2 \frac{C_R}{C_V^2}$
$C_{Ls}$	lift coefficient based on principal wetted area, $\frac{\Delta}{\rho V^2 s} = \frac{C_{Lb}}{l_m/b}$
$C_{Ds}$	drag coefficient based on principal wetted area, $\frac{R}{\rho V^2 s} = \frac{C_{D_b}}{l_m/b}$
$\beta$	angle of dead rise, deg
$\rho$	mass density of water, slugs/ft <sup>3</sup>
$\tau$	trim (angle between keel and horizontal), deg
$\nu$	kinematic viscosity, ft <sup>2</sup> /sec

#### DESCRIPTION OF THE MODELS

The models are simple V-shaped prismatic surfaces having angles of dead rise of 20° and 40°, as shown in figures 1 and 2, respectively. Each model is constructed of brass, has a rectangular plan form and a beam of 4 inches, and is 36 inches long. A detailed description of the construction and finish of the models is presented in reference 1.

#### APPARATUS AND PROCEDURES

A description of the Langley tank no. 1, the apparatus for towing the model, and the instrumentation for measuring the lift, drag, and

trimming moment are given in reference 3, and the general procedure for making the tests is given in reference 1. A diagram of the model and towing gear is presented in figure 3.

The wetted lengths were usually obtained from underwater photographs, and when photographs were not available, visual readings were used. A typical underwater photograph of the V-shaped surface is shown in figure 4. The mean wetted length was taken as the average of the keel and chine wetted lengths. Actually, as can be seen in figure 4, the visible stagnation line appears to be slightly curved so that the actual mean wetted length is slightly greater than the average of the keel and chine wetted lengths. The difference, however, was generally within the precision of measurement and therefore was neglected in the calculation of the mean wetted length and the principal wetted area.

A similar underwater photograph of a surface having an 8-inch beam and a  $20^{\circ}$  angle of dead rise is shown in figure 5. The wool tufts attached to the bottom of the model show in more detail the change in flow at the visible stagnation line used to define the principal wetted area. Forward of the stagnation line, the flow is seen to be principally in a lateral direction and consists primarily of light spray which contributes little or no lift. Behind this line, the flow is toward the trailing edge with a small lateral component near the chines.

Only a limited number of draft data were obtained since the apparatus, described in reference 2, for measuring the water level was not available during most of the tests.

The aerodynamic tares were held to a minimum by the wind-shielding arrangement described in reference 1. The force data were corrected for any residual tares that were appreciable. The quantities measured are generally believed to be accurate within the following limits:

Load, lb . . . . .	±0.15
Trim, deg . . . . .	±0.10
Speed, ft/sec . . . . .	±0.20
Resistance, lb . . . . .	±0.15
Trimming moment, ft-lb . . . . .	±0.50
Wetted length, in. . . . .	±0.25

## RESULTS

The experimental data for the surface having an angle of dead rise of  $20^{\circ}$  are presented in table I and those for the surface having an angle of dead rise of  $40^{\circ}$ , in table II. The load, resistance, speed, wetted lengths, and center-of-pressure location are expressed as conventional

nondimensional hydrodynamic coefficients. By following the procedure used in references 1 and 2, the lift and drag coefficients are expressed both in terms of the square of the beam and in terms of the principal wetted area. The draft data are limited in scope and have therefore been omitted from the tables of data. Data for the dry-chine condition were also omitted inasmuch as the precision of the data for this condition became marginal because of the small wetted areas. The nonplaning conditions, those conditions strongly affected by buoyancy, for the surface having a 20° angle of dead rise were not included herein in light of the results of the supplementary low-speed schedule described in reference 1. For the surface having a 40° angle of dead rise, all conditions where buoyancy exceeded 20 percent of the total load (ref. 2) were considered nonplaning and were not included.

Plots of the data are presented in figures 6 to 19. In general, the trends with dead rise are the same as those noted in reference 2. With an increase in the angle of dead rise, the wetted length (or area) required at a given lift coefficient and trim was increased. (See figs. 6 and 7.) The difference between the keel and chine wetted lengths was constant for a given trim for both models (figs. 8 and 9). This difference (fig. 10) was greater for the model with the higher angle of dead rise and showed the same trends as those predicted by the two-dimensional wave-rise theory of Wagner as applied in reference 4. The experimental values are generally lower than those given by theory and the differences are generally greater for the surface having the higher angle of dead rise.

For a given value of  $C_{Lb}$ , an increase in angle of dead rise resulted in a forward shift of the center-of-pressure location (figs. 11 and 12). The average ratio of  $l_p/l_m$  for each trim is presented in figures 13 and 14. Increasing the angle of dead rise decreases this ratio as can be seen in figure 15 in which the variation of  $l_p/l_m$  with trim is shown for both surfaces.

Draft data for the two models are shown in figures 16 and 17 where the measured draft in beams is plotted against that computed from the keel wetted length. The computed draft is defined by  $\frac{l_k}{b} \sin \tau$ . These data show evidence of pile-up of water at the keel for both models at high trims. The amount of pile-up generally appears to be least for the surface having the higher angle of dead rise.

Figures 18 and 19 present the total drag and the induced drag computed from the lift where the induced drag coefficient is defined by  $C_{Lb} \tan \tau$ . The difference between the measured drag and the induced drag is the friction drag. Comparison of these figures indicates that the increase in angle of dead rise results in an increase in friction

drag for a given lift coefficient because of the greater wetted area. At the higher trims, the friction-drag component is small or negligible as compared with the induced-drag component.

The calculated skin-friction coefficients for trims where the friction is appreciable are plotted against Reynolds number in figures 20 and 21. In calculating the skin-friction coefficients from the test data, the values obtained from faired curves of total drag coefficient (figs. 18 and 19) and the values obtained from faired curves of mean-wetted-length-beam ratio (figs. 6 and 7) were used to improve the precision. The grouping of the data with respect to the Schoenherr and Blasius lines suggests that the boundary layer at the higher Reynolds numbers was fully turbulent and that the friction at larger scales may be calculated with reasonable accuracy from the Schoenherr line (ref. 5).

#### CONCLUDING REMARKS

The effects of an increase in angle of dead rise on the planing characteristics of a prismatic surface are, in general, those that would be expected from a consideration of the change in geometry caused by a change in the angle of dead rise. For a given condition of load, speed, and trim, an increase in angle of dead rise increased the wetted length and hydrodynamic resistance and moved the center-of-pressure location forward. These results are also consistent with those obtained in an investigation of the effects of increasing the angle of dead rise on the planing characteristics of prismatic surfaces having horizontally flared chines (NACA TN's 2804 and 2842).

Langley Aeronautical Laboratory,  
National Advisory Committee for Aeronautics,  
Langley Field, Va., October 22, 1952.

## REFERENCES

1. Kapryan, Walter J., and Weinstein, Irving: The Planing Characteristics of a Surface Having a Basic Angle of Dead Rise of  $20^{\circ}$  and Horizontal Chine Flare. NACA TN 2804, 1952.
2. Blanchard, Ulysse J.: The Planing Characteristics of a Surface Having a Basic Angle of Dead Rise of  $40^{\circ}$  and Horizontal Chine Flare. NACA TN 2842, 1952.
3. Truscott, Starr: The Enlarged N.A.C.A. Tank, and Some of Its Work. NACA TM 918, 1939.
4. Korvin-Kroukovsky, B. V., Savitsky, Daniel, and Lehman, William F.: Wetted Area and Center of Pressure of Planing Surfaces. Preprint No. 244, S.M.F. Fund Paper, Inst. Aero. Sci. (Rep. No. 360, Project No. NR062-012, Office Naval Res., Exp. Towing Tank, Stevens Inst. Tech., Aug. 1949.)
5. Davidson, Kenneth S. M.: Resistance and Powering. Detailed Considerations - Skin Friction. Vol. II of Principles of Naval Architecture, ch. II, pt. 2, sec. 7, Henry E. Rossell and Lawrence B. Chapman, eds., Soc. Naval Arch. and Marine Eng., 1939, pp. 76-83.







TABLE I - Concluded

EXPERIMENTAL DATA OBTAINED FOR A PLANING SURFACE HAVING A 20° ANGLE OF DEAD RISE  
LANGLEY TANK MODEL 276

Trim, $\tau$ , deg	$c_A$	$c_V$	$c_R$	$\frac{t_c}{b}$	$\frac{t_{lb}}{b}$	$\frac{t_k}{b}$	$\frac{t_p}{b}$	$c_{L_D}$	$c_{D_b}$	$c_{L_S}$	$c_{D_S}$
30	10.65	11.19	6.10	0.32	0.39	0.45	0.06	0.1701	0.0974	0.436	0.2497
30	10.65	16.26	5.87	---	---	---	---	.0806	.0444	---	---
30	19.17	8.72	11.18	1.30	1.36	1.42	.78	.5042	.2940	.371	.2162
30	19.17	9.70	10.97	.98	1.04	1.10	.60	.4075	.2330	.392	.2240
30	19.17	9.76	11.12	1.00	1.06	1.12	.60	.4025	.2350	.380	.2217
30	19.17	12.47	10.83	.50	.57	.65	.33	.2466	.1395	.433	.2447
30	19.17	17.48	10.66	.18	.28	.38	.18	.1255	.0696	.448	.2486
30	19.17	21.94	10.58	.12	.19	.25	.18	.0804	.0444	.423	.2337
30	27.69	15.10	15.75	.50	.56	.62	.39	.2429	.1380	.434	.2464
30	27.69	17.75	15.80	.35	.41	.48	.30	.1758	.1005	.429	.2451
30	27.69	21.35	15.69	.12	.21	.30	.24	.1215	.0689	.579	.3281
30	27.69	25.32	15.62	0	.06	.12	.21	.0865	.0487	1.442	.8117
30	36.21	12.20	20.88	1.28	1.34	1.40	.94	.4866	.2810	.363	.2097
30	36.21	14.94	20.95	.75	.81	.87	.48	.3245	.1870	.401	.2309
30	36.21	15.10	20.74	.72	.79	.85	.45	.3176	.1820	.402	.2304
30	36.21	15.13	21.09	.78	.85	.92	.45	.3164	.1830	.372	.2153
30	36.21	15.25	20.68	.75	.81	.88	.48	.3114	.1778	.384	.2195
30	36.21	20.01	20.65	.32	.39	.45	.18	.1810	.1030	.464	.2641
30	36.21	20.13	20.94	.32	.41	.50	.21	.1790	.1030	.437	.2512
30	36.21	20.19	21.07	.32	.39	.45	.24	.1777	.1035	.456	.2654
30	36.21	24.71	20.29	.12	.19	.25	.21	.1186	.0667	.624	.3511
30	36.21	24.86	20.33	.12	.19	.25	.30	.1172	.0674	.617	.3547
30	53.25	14.61	30.50	1.32	1.39	1.45	.84	.4989	.2860	.359	.2058
30	53.25	16.20	30.63	.98	1.04	1.10	.63	.4058	.2340	.390	.2250
30	53.25	18.30	30.65	.75	.81	.88	.45	.3180	.1830	.393	.2259
30	53.25	20.98	30.55	.50	.56	.62	.30	.2420	.1388	.432	.2479
30	53.25	24.28	30.45	.32	.39	.45	.12	.1807	.1030	.463	.2641
30	53.25	25.22	30.50	.25	.31	.38	.23	.1674	.0960	.540	.3097









TABLE II - Concluded

EXPERIMENTAL DATA OBTAINED FOR A PLANING SURFACE HAVING A  $40^{\circ}$  ANGLE OF DEAD RISE  
 LANGLEY TANK MODEL 277

Trim, $\tau$ , deg	$C_D$	$C_V$	$C_R$	$\frac{i_c}{b}$	$\frac{i_m}{b}$	$\frac{i_k}{b}$	$\frac{i_p}{b}$	$C_{L_b}$	$.C_{D_b}$	$C_{L_s}$	$C_{D_s}$
30	27.69	21.14	16.35	0.30	0.50	0.70	0.24	0.1240	0.0732	0.2480	0.1464
30	27.69	21.35	16.35	.18	.31	.45	.24	.1215	.0716	.3919	.2310
30	27.69	24.49	16.30	.12	.32	.52	.20	.0924	.0544	.2888	.1700
30	36.21	12.11	21.51	1.95	2.05	2.15	1.20	.4938	.2934	.2409	.1431
30	36.21	12.11	21.45	1.88	2.00	2.12	1.17	.4938	.2925	.2469	.1462
30	36.21	12.14	21.36	1.90	2.04	2.18	1.14	.4914	.2899	.2409	.1421
30	36.21	15.07	21.45	1.15	1.26	1.38	.69	.3189	.1889	.2531	.1499
30	36.21	15.25	21.39	1.10	1.25	1.40	.69	.3114	.1840	.2491	.1472
30	36.21	17.23	21.52	.80	.95	1.10	.42	.2439	.1448	.2567	.1524
30	36.21	19.86	21.42	.52	.68	.82	.38	.1836	.1086	.2700	.1597
30	36.21	20.13	21.11	.55	.70	.85	.30	.1788	.1040	.2554	.1486
30	36.21	24.25	21.48	.25	.52	.80	.15	.1230	.0730	.2385	.1404
30	36.21	25.25	21.75	.20	.39	.58	.22	.1136	.0680	.2913	.1744
30	53.25	14.79	31.37	1.92	2.02	2.12	1.11	.4869	.2866	.2410	.1419
30	53.25	16.29	31.28	1.55	1.70	1.85	.90	.4014	.2358	.2361	.1387
30	53.25	16.41	31.41	1.52	1.62	1.72	.87	.3955	.2333	.2441	.1440
30	53.25	20.83	31.26	.62	.78	.92	.51	.2454	.1441	.3146	.1847
30	53.25	25.44	31.67	.60	.75	.90	.27	.1648	.0979	.2197	.1309
30	70.29	16.87	41.50	2.12	2.27	2.42	1.17	.4940	.2918	.2176	.1285
30	70.29	20.98	41.36	1.20	1.35	1.50	.72	.3194	.1879	.2366	.1392
30	70.29	22.51	40.73	.95	1.10	1.25	.54	.2774	.1607	.2522	.1461
30	70.29	22.69	41.15	.98	1.14	1.30	.60	.2730	.1599	.2395	.1403
30	70.29	24.95	41.30	.72	.87	1.02	.46	.2258	.1327	.2595	.1525
30	70.29	25.01	41.33	.80	.94	1.08	.47	.2247	.1322	.2390	.1406
30	87.33	18.60	52.00	2.00	2.15	2.30	1.23	.5048	.3006	.2348	.1398
30	87.33	18.70	51.31	1.98	2.12	2.28	1.23	.4995	.2934	.2356	.1384
30	87.33	18.70	51.29	1.95	2.09	2.22	1.23	.4995	.2934	.2390	.1404
30	87.33	21.04	51.19	1.62	1.78	1.92	.93	.3946	.2313	.2217	.1299
30	87.33	22.88	50.99	1.12	1.28	1.42	.66	.3336	.1948	.2606	.1522
30	87.33	25.22	51.32	.88	1.03	1.18	.58	.2746	.1614	.2666	.1567



NACA TN 2876

16

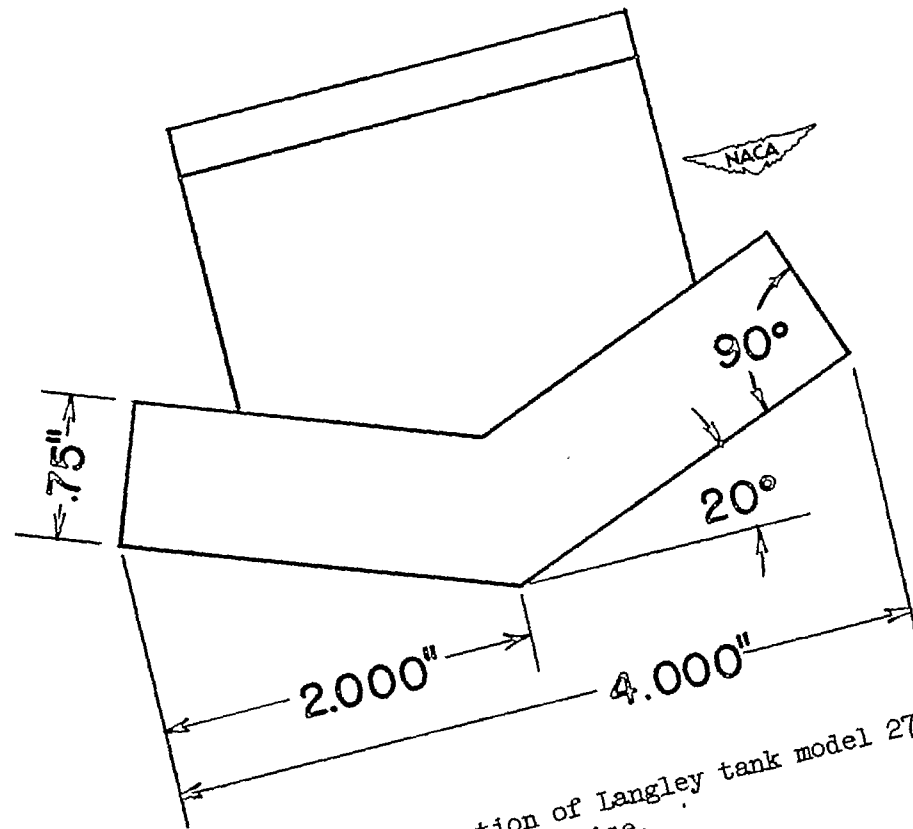
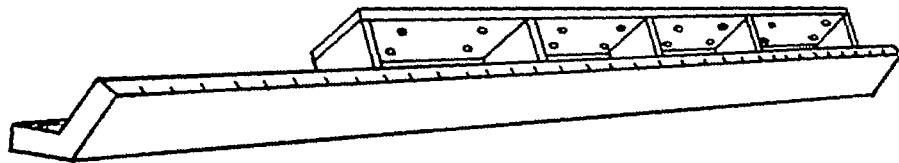


Figure 1.- Sketch and cross section of Langley tank model 276, 20° angle of dead rise.

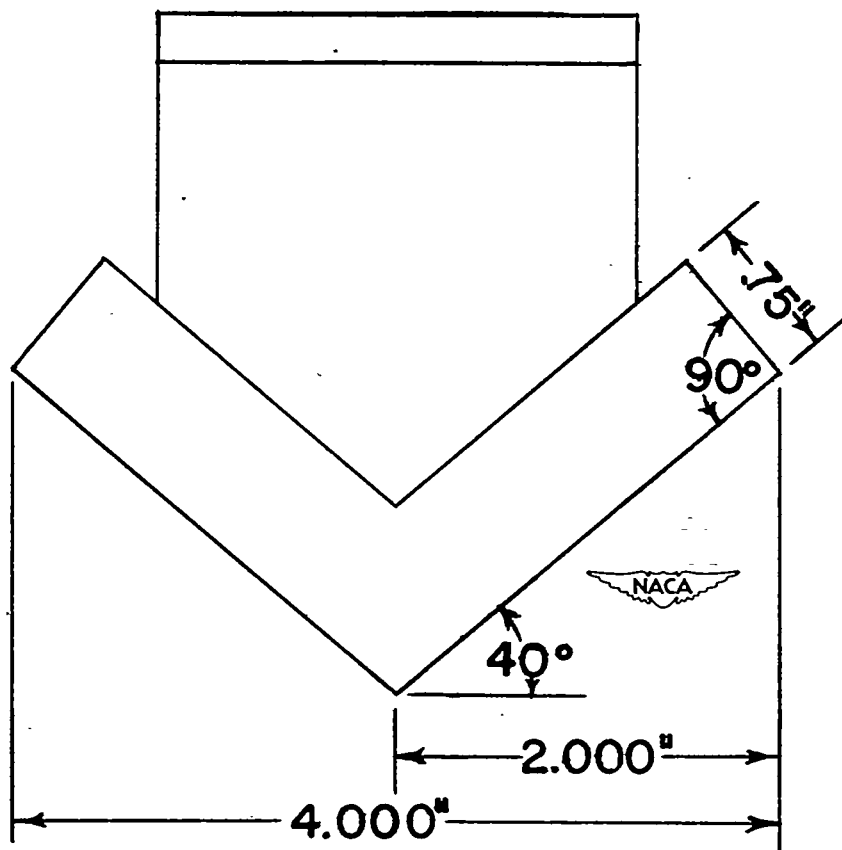
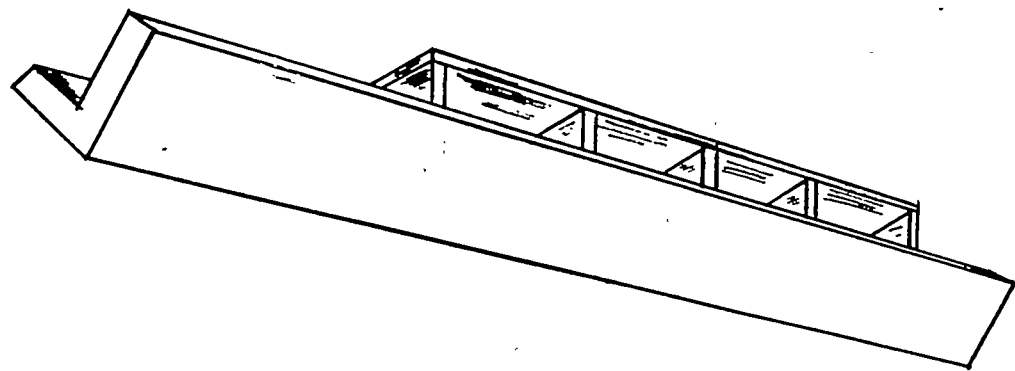


Figure 2.- Sketch and cross section of Langley tank model 277,  $40^\circ$  angle of dead rise.

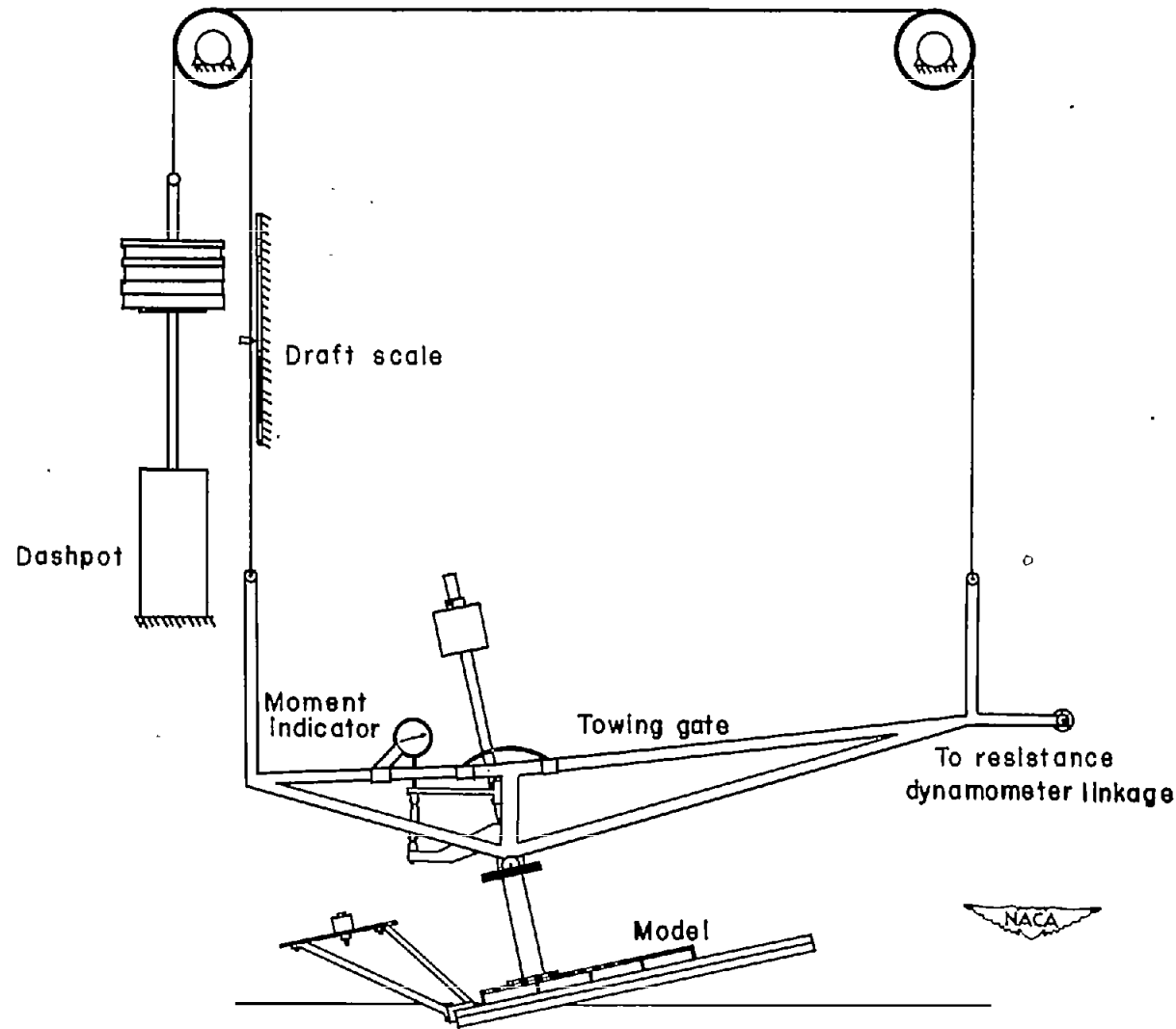


Figure 3.- Setup of model and towing gear.

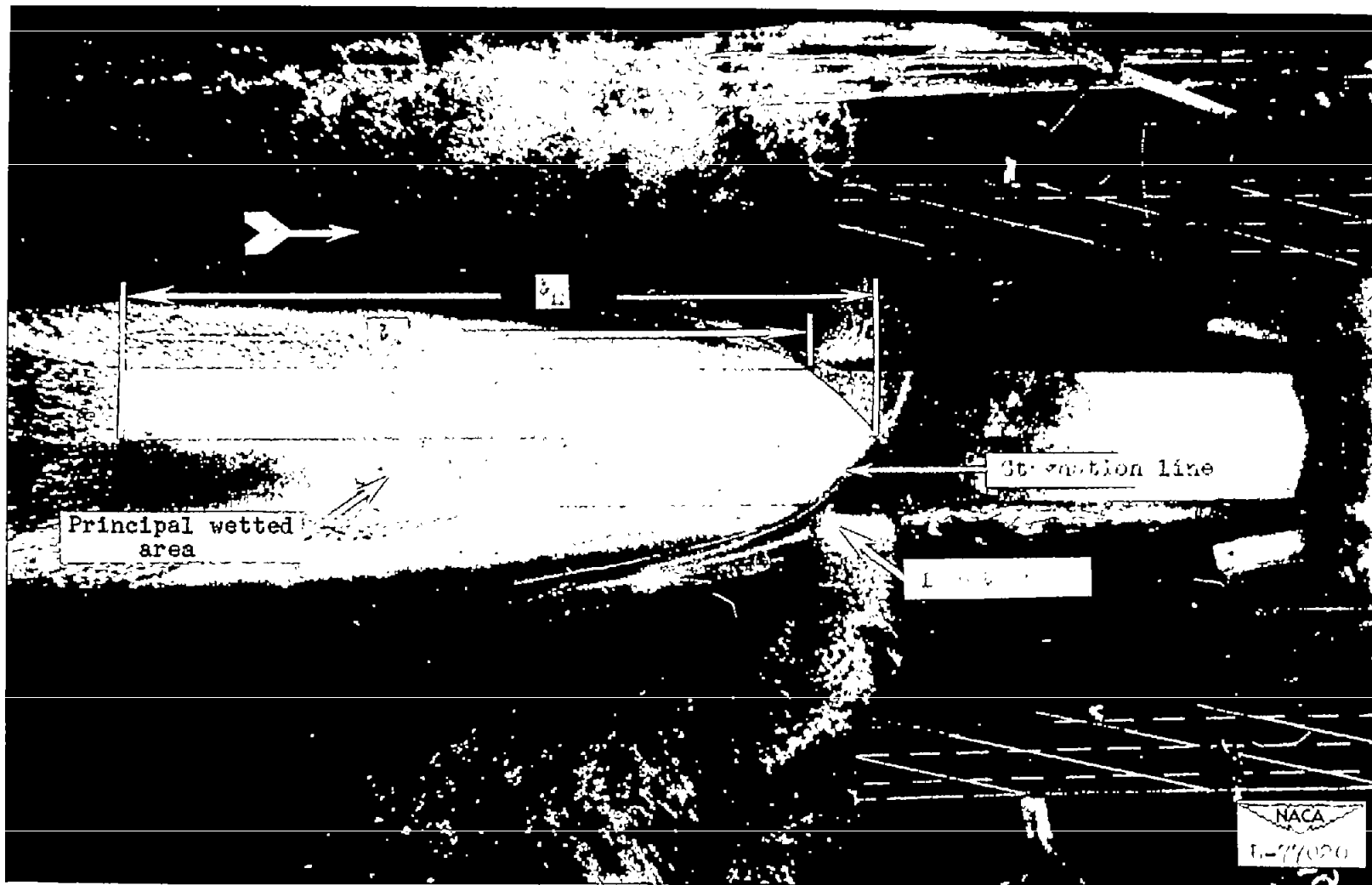


Figure 4.- Typical underwater photograph.

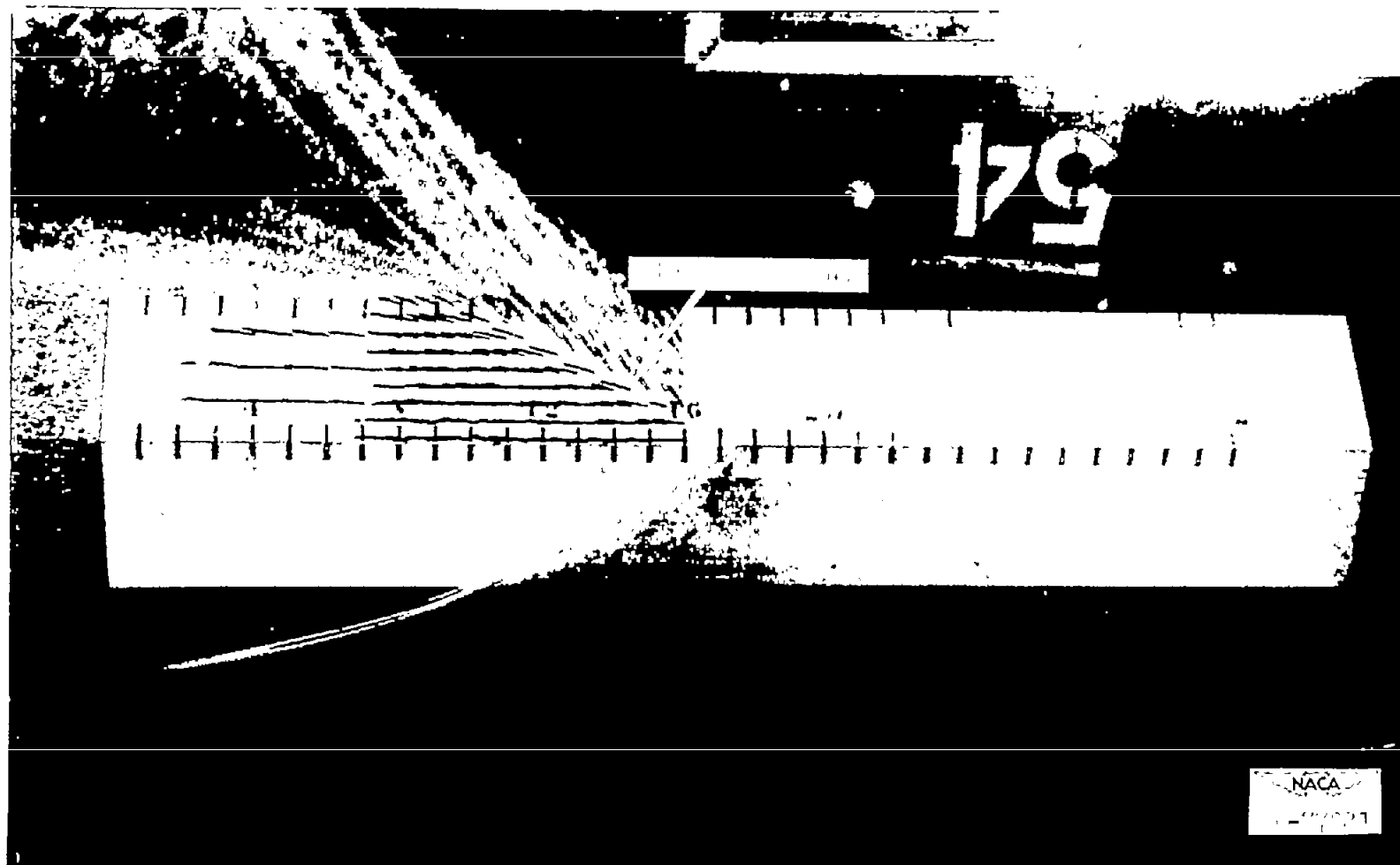


Figure 5.- Typical flow pattern for a V-shaped surface having a  $20^{\circ}$  angle of dead rise.

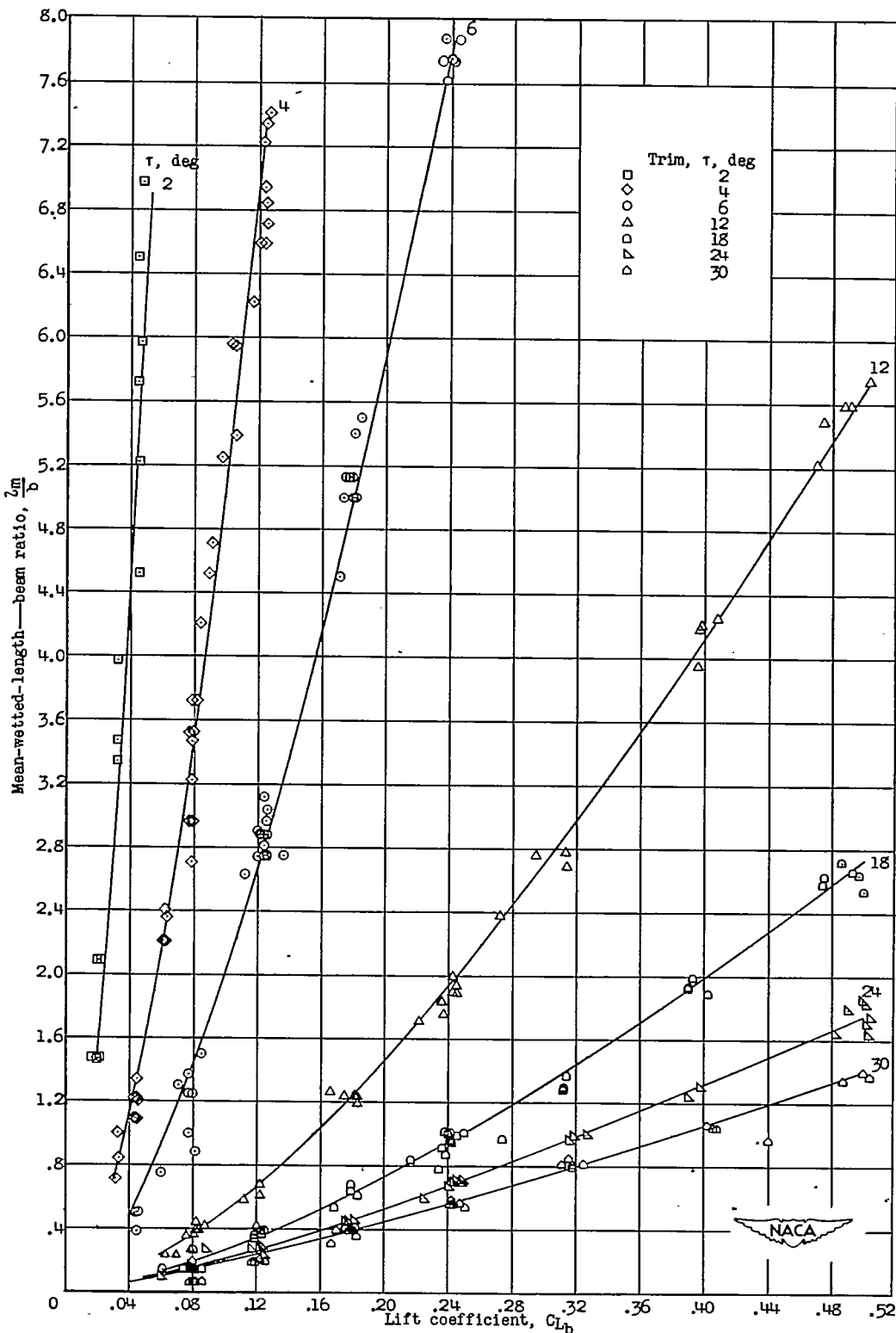


Figure 6.- Variation of mean-wetted-length-beam ratio with lift coefficient for surface having a 20° angle of dead rise.

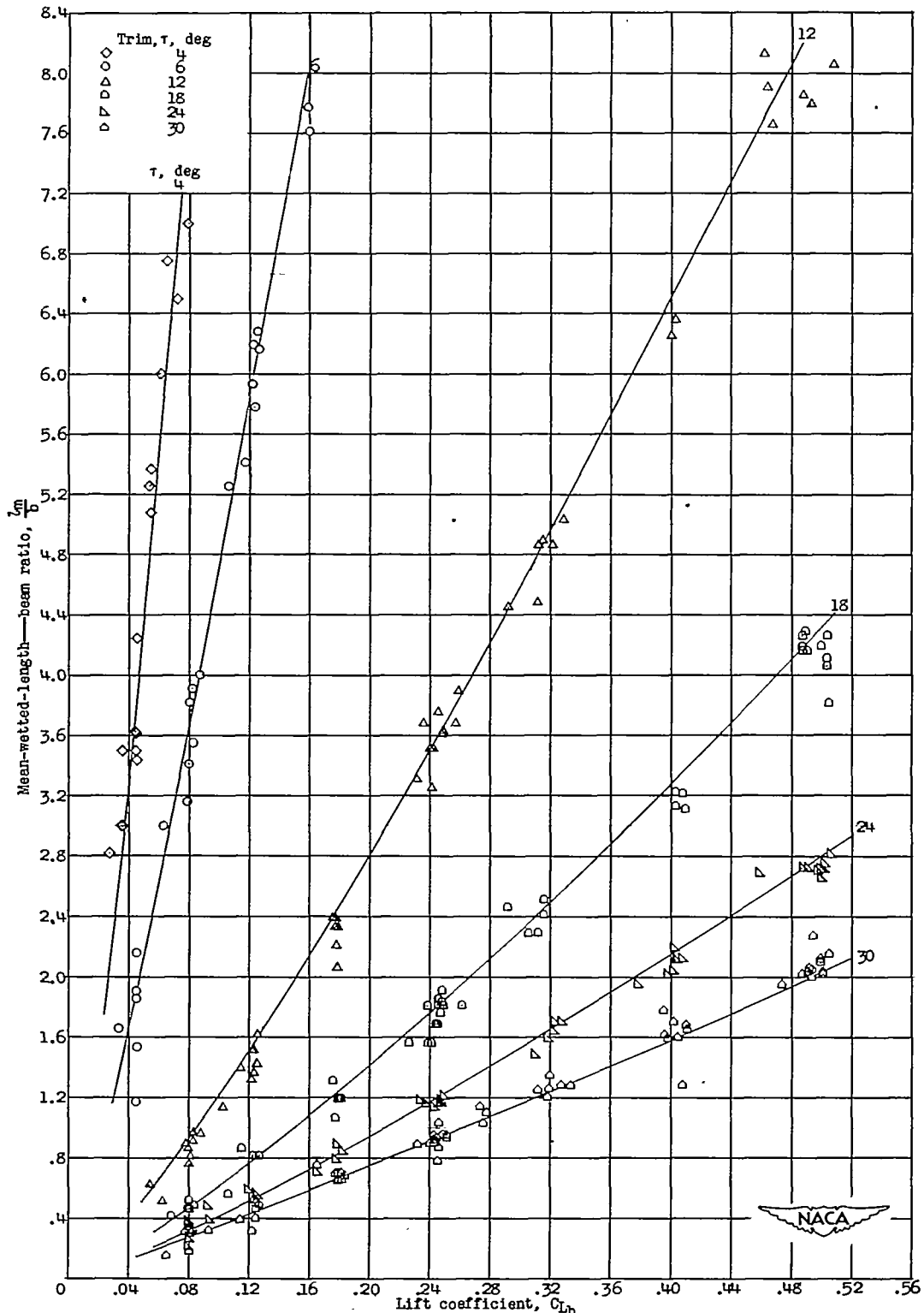


Figure 7.- Variation of mean-wetted-length-beam ratio with lift coefficient for surface having a  $40^\circ$  angle of dead rise.

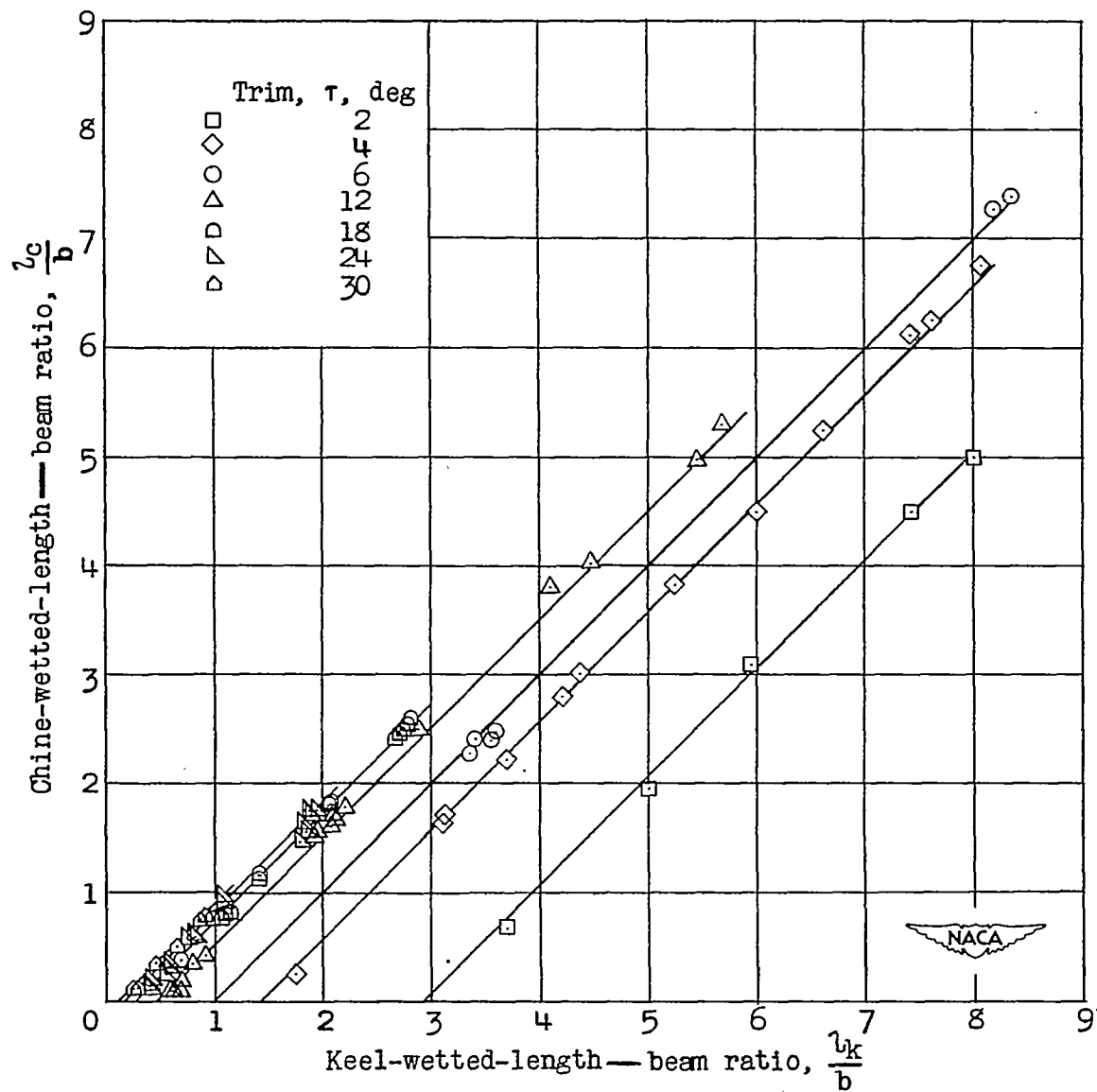


Figure 8.- Variation of chine-wetted-length-beam ratio with keel-wetted-length-beam ratio for surface having a 20° angle of dead rise.

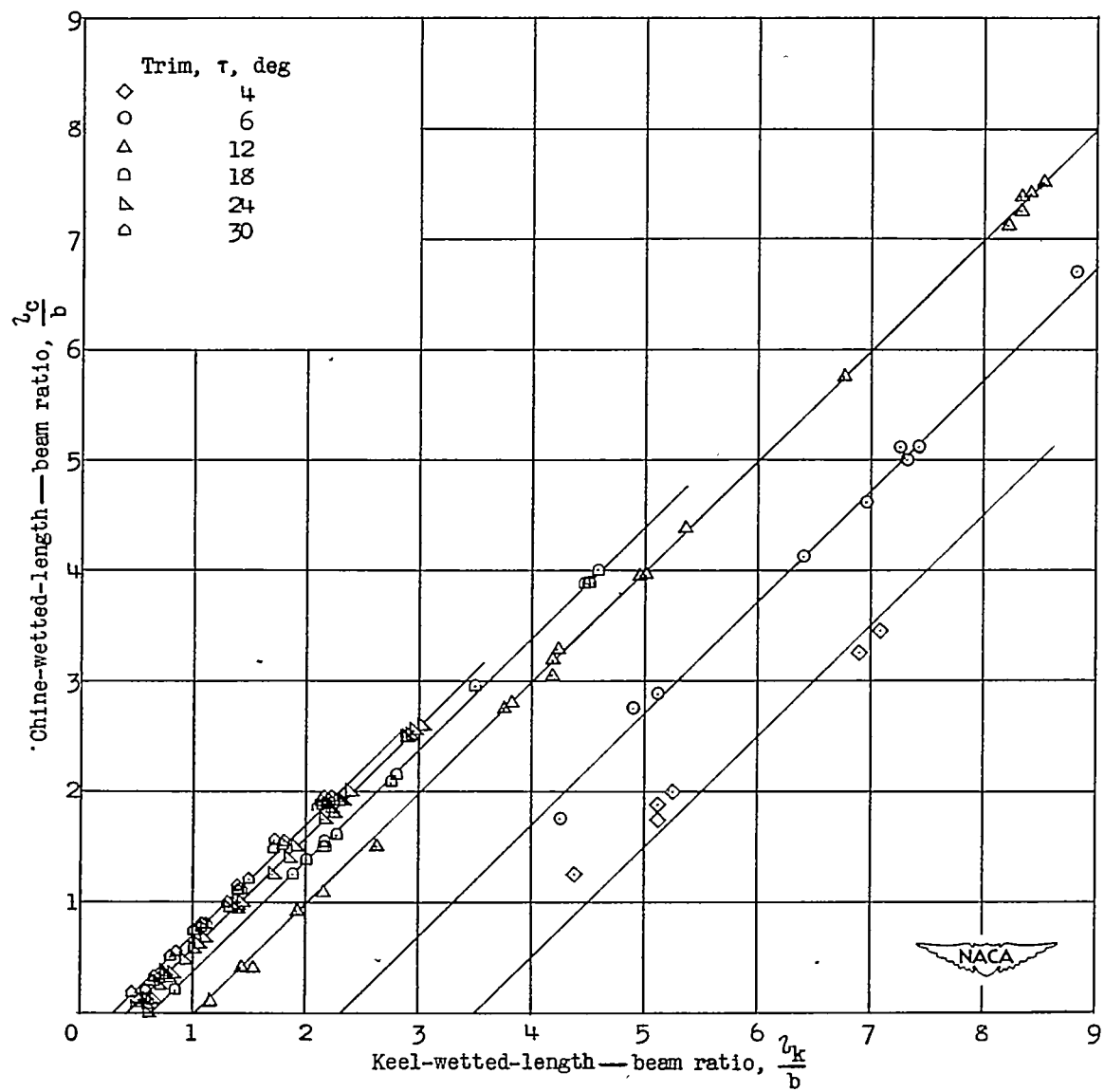


Figure 9.- Variation of chine-wetted-length-beam ratio with keel-wetted-length-beam ratio for surface having a  $40^\circ$  angle of dead rise.

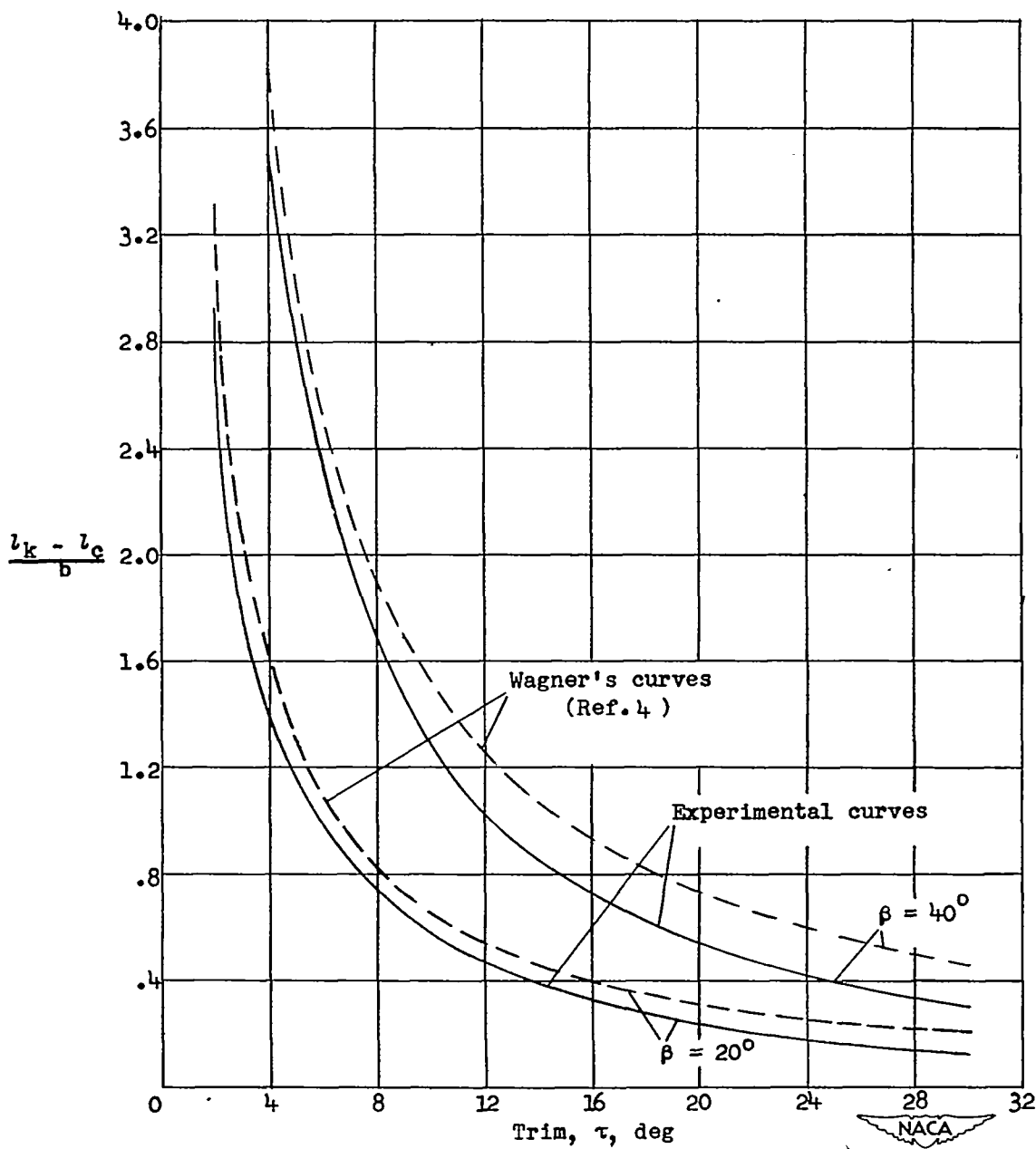


Figure 10.- Variation of  $\frac{l_k - l_c}{b}$  with trim.

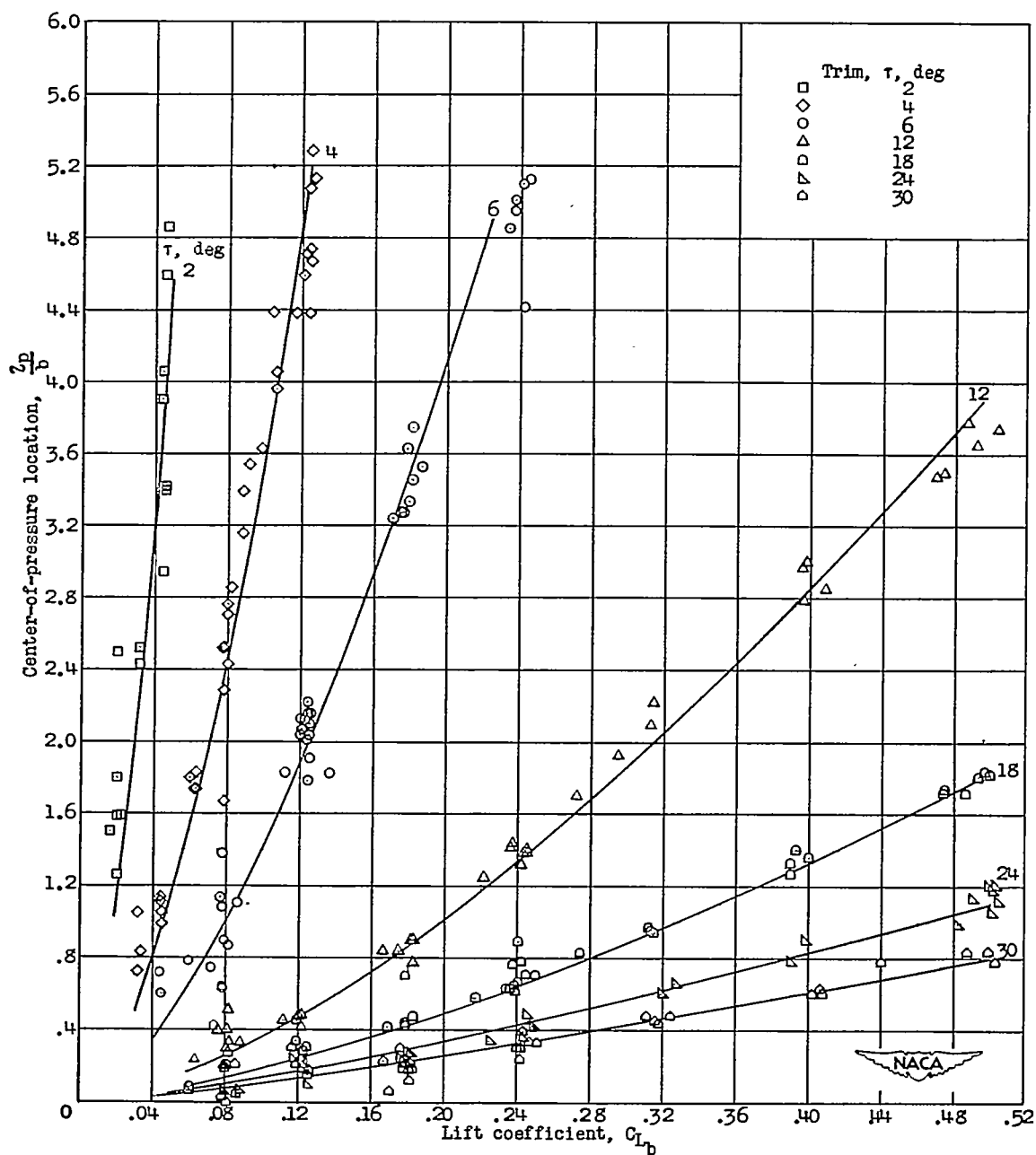


Figure 11.- Variation of center-of-pressure location with lift coefficient for surface having a  $20^\circ$  angle of dead rise.

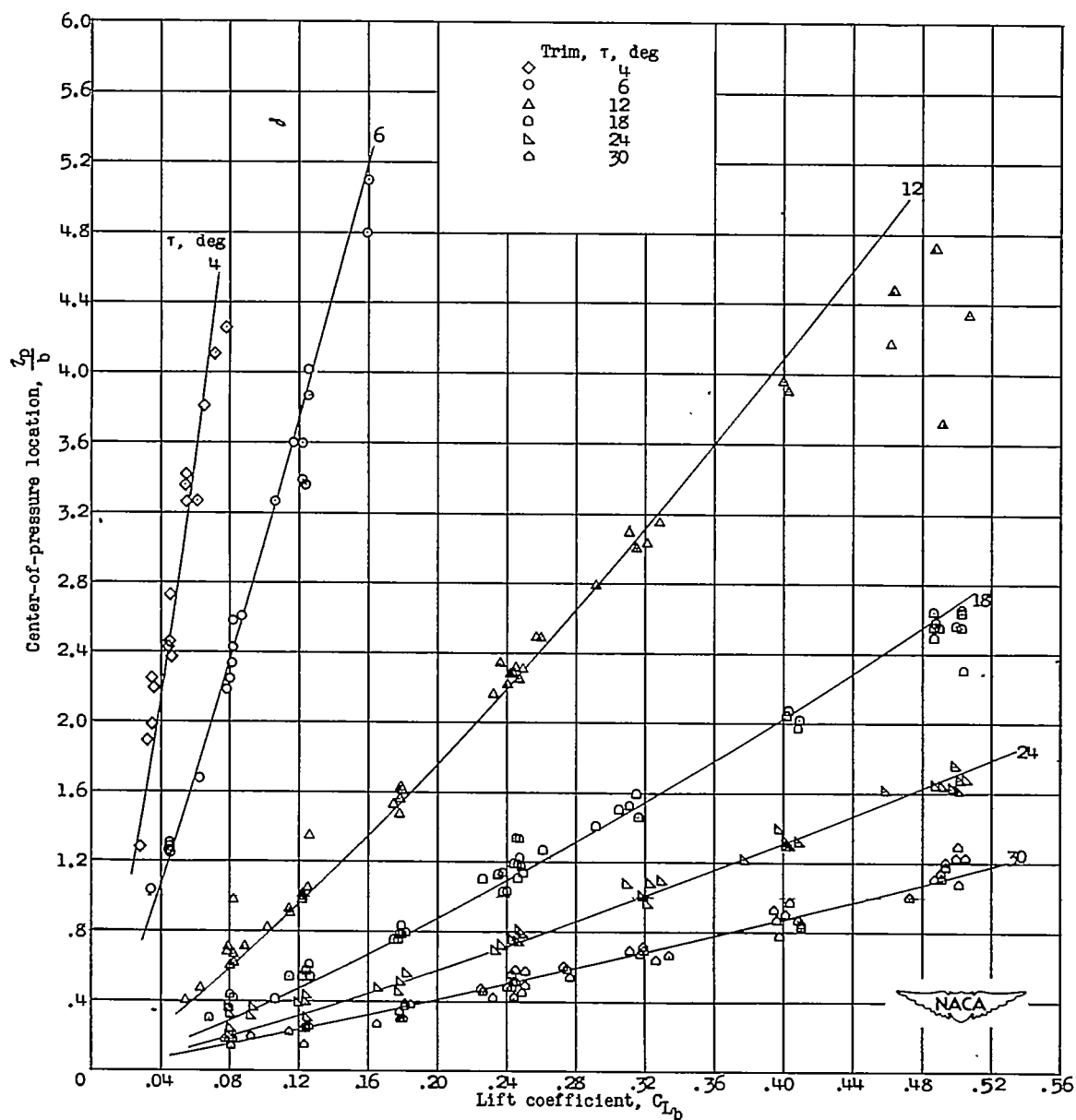


Figure 12.- Variation of center-of-pressure location with lift coefficient for surface having a  $40^{\circ}$  angle of dead rise.

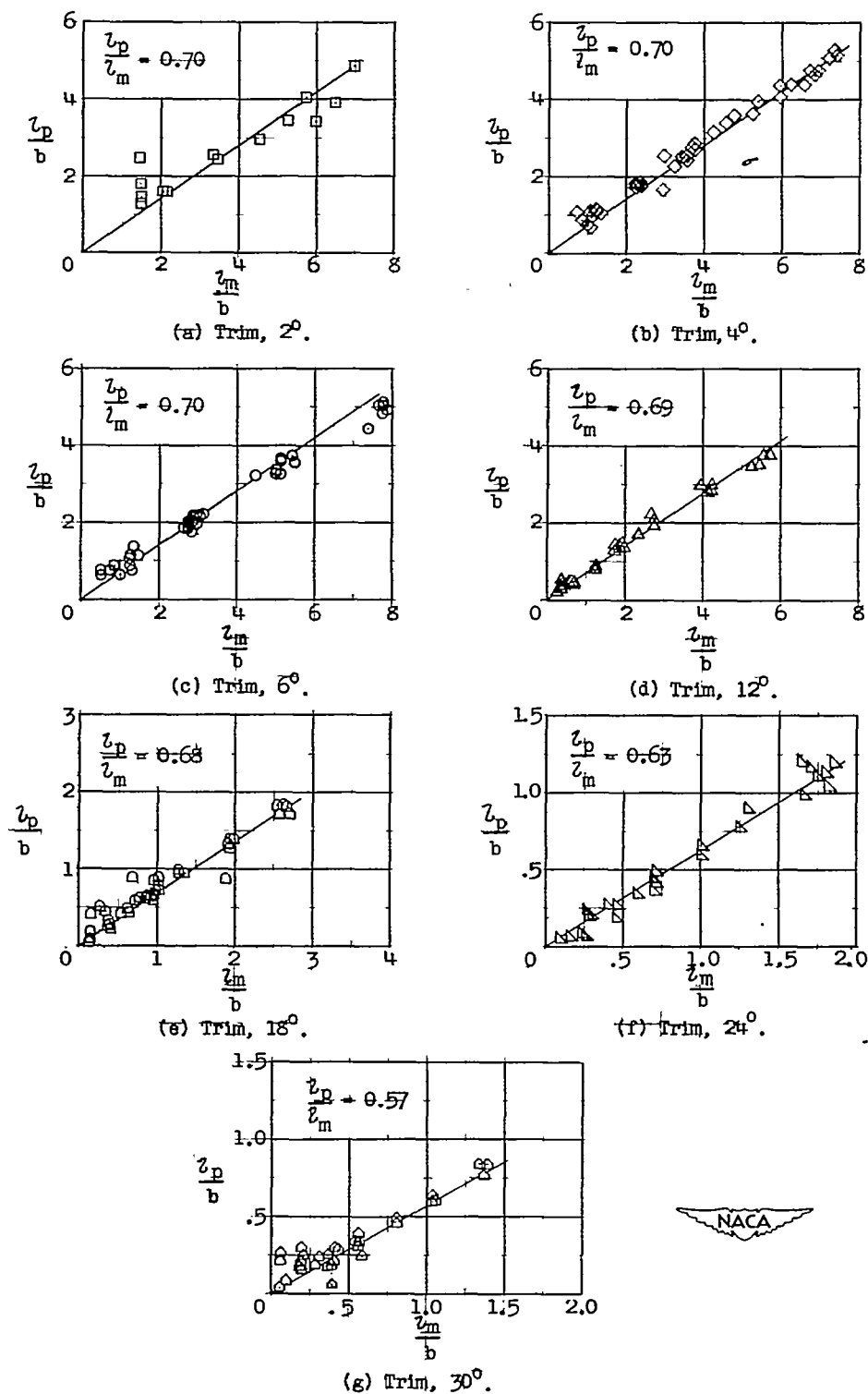


Figure 13.- Variation of  $\frac{l_p}{b}$  with  $\frac{l_m}{b}$  for surface having a  $20^\circ$  angle of dead rise.

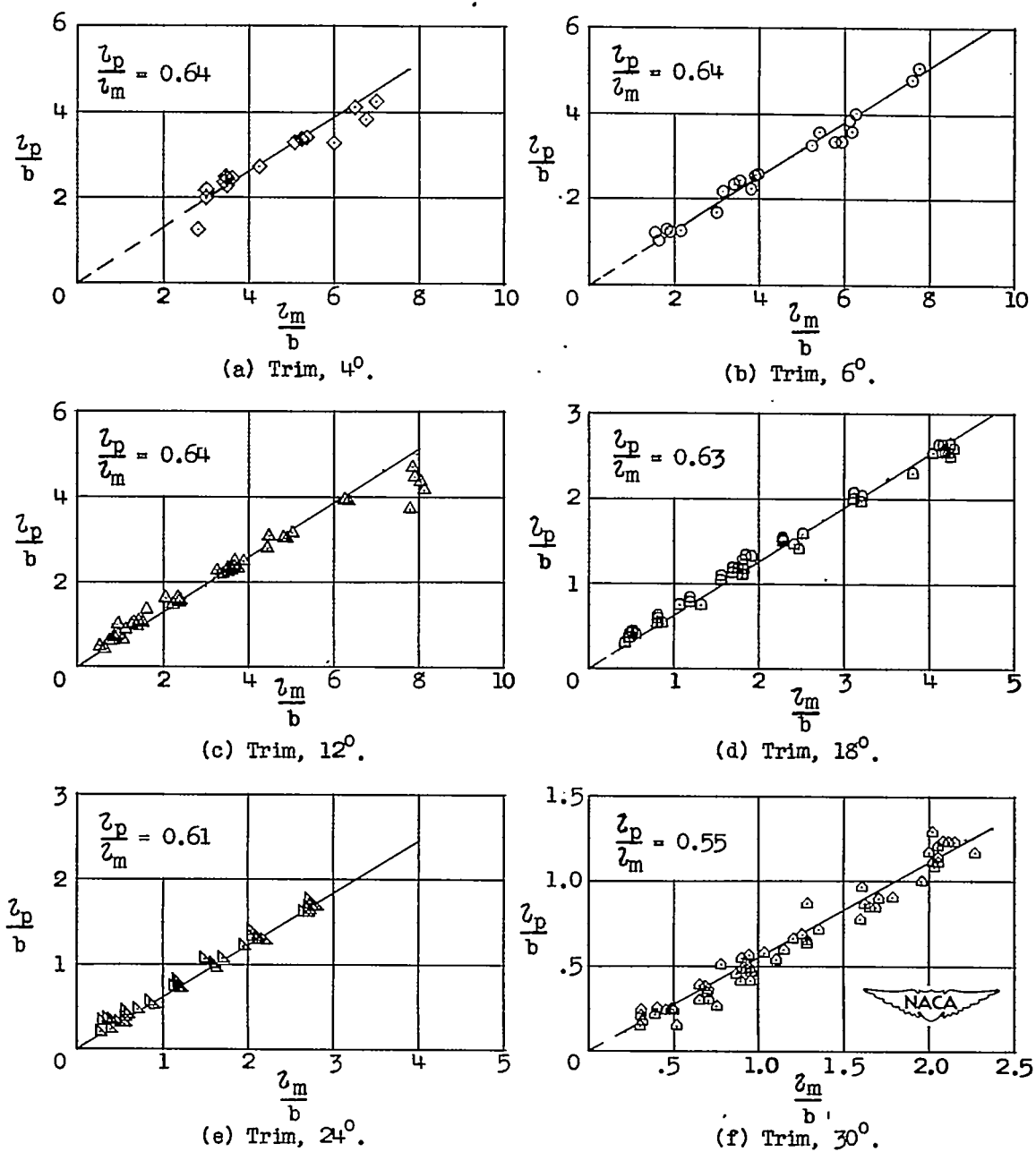


Figure 14.- Variation of  $\frac{l_p}{b}$  with  $\frac{l_m}{b}$  for surface having a  $40^0$  angle of dead rise.

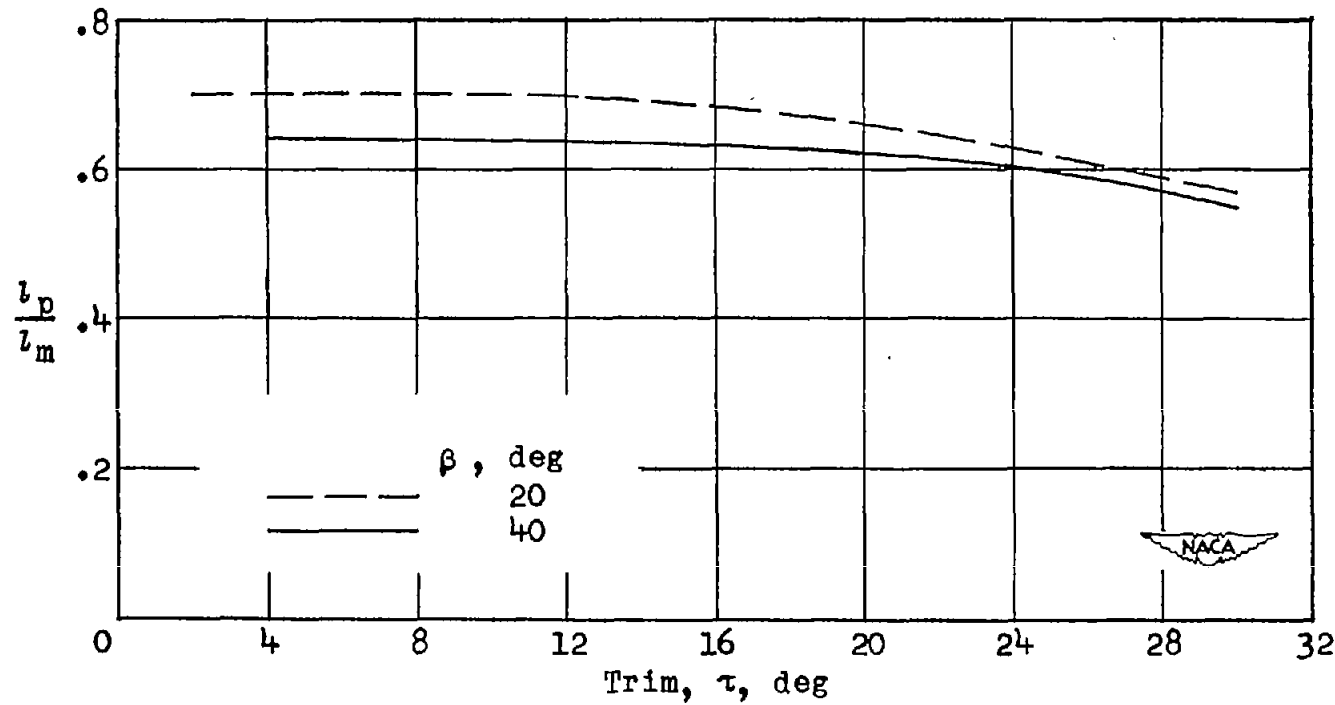


Figure 15.- Comparison of variation of  $\frac{l_p}{l_m}$  with trim for surfaces having 20° and 40° angles of dead rise.

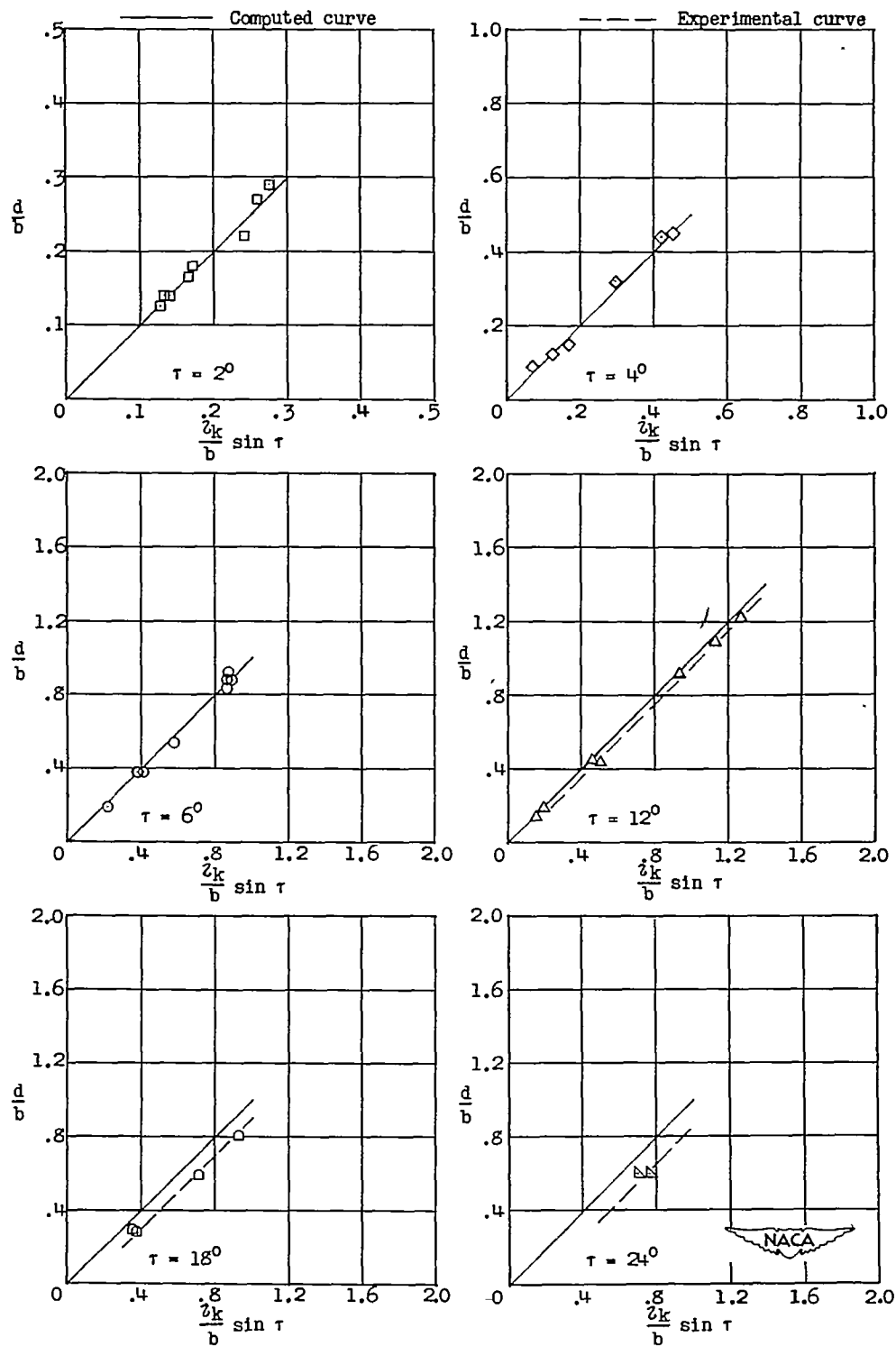


Figure 16.- Comparison of experimental draft data with computed draft data showing pile-up at the keel for surface having a  $20^{\circ}$  angle of dead rise.

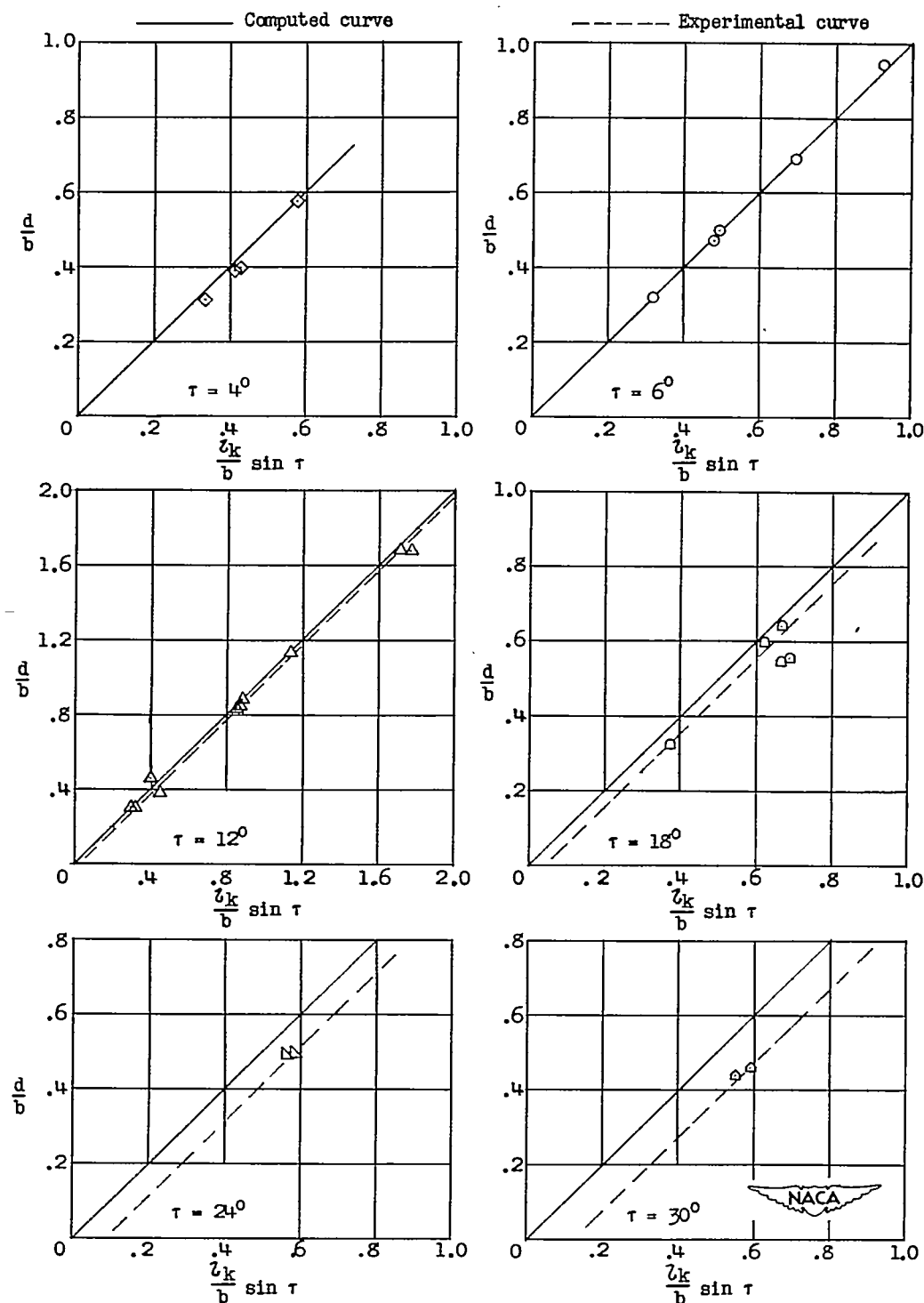


Figure 17.- Comparison of experimental draft data with computed draft data showing pile-up at the keel for surface having a  $40^0$  angle of dead rise.

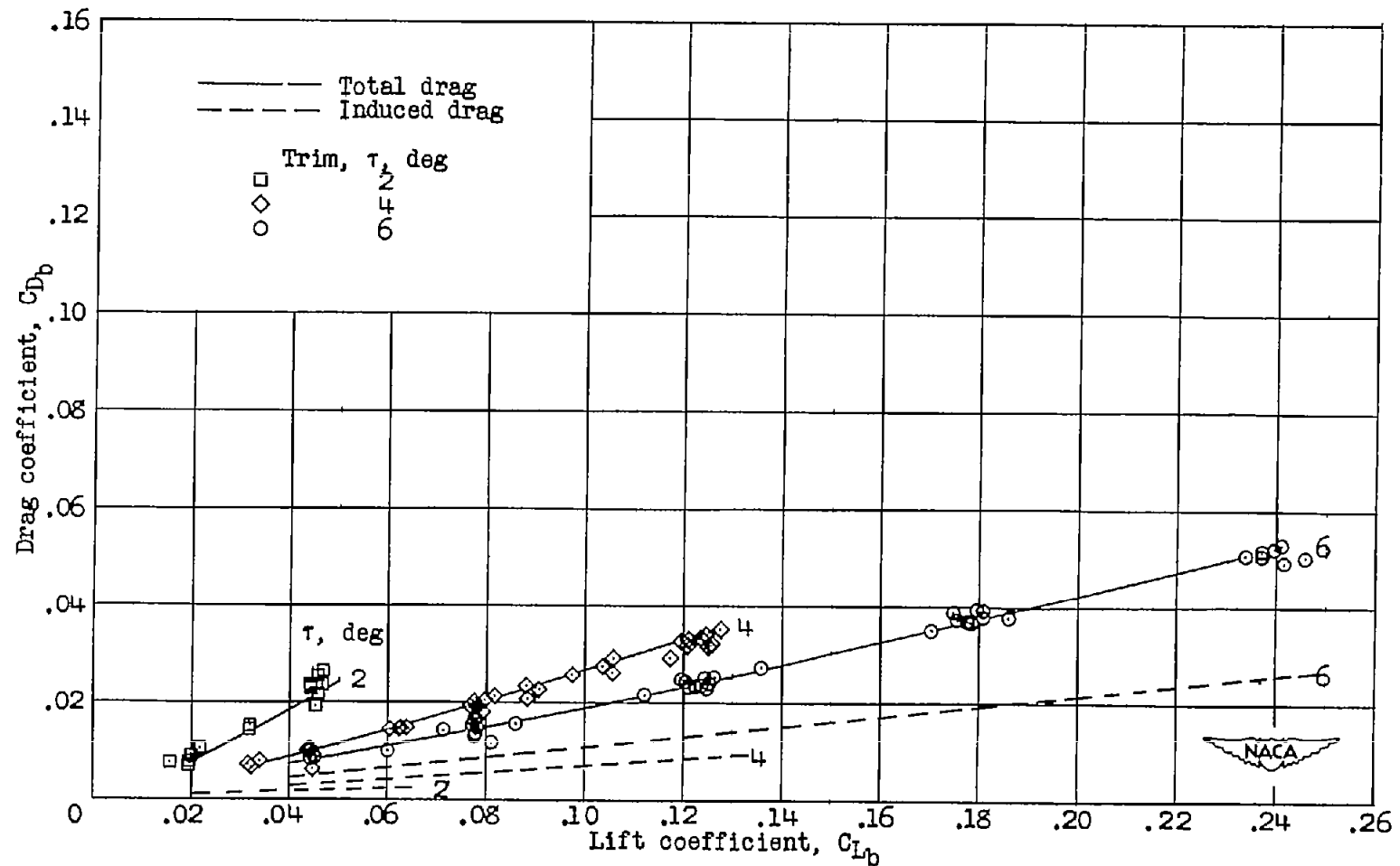
(a) Trim,  $2^\circ$ ,  $4^\circ$ , and  $6^\circ$ .

Figure 18.- Variation of drag coefficient with lift coefficient for surface having a  $20^\circ$  angle of dead rise.

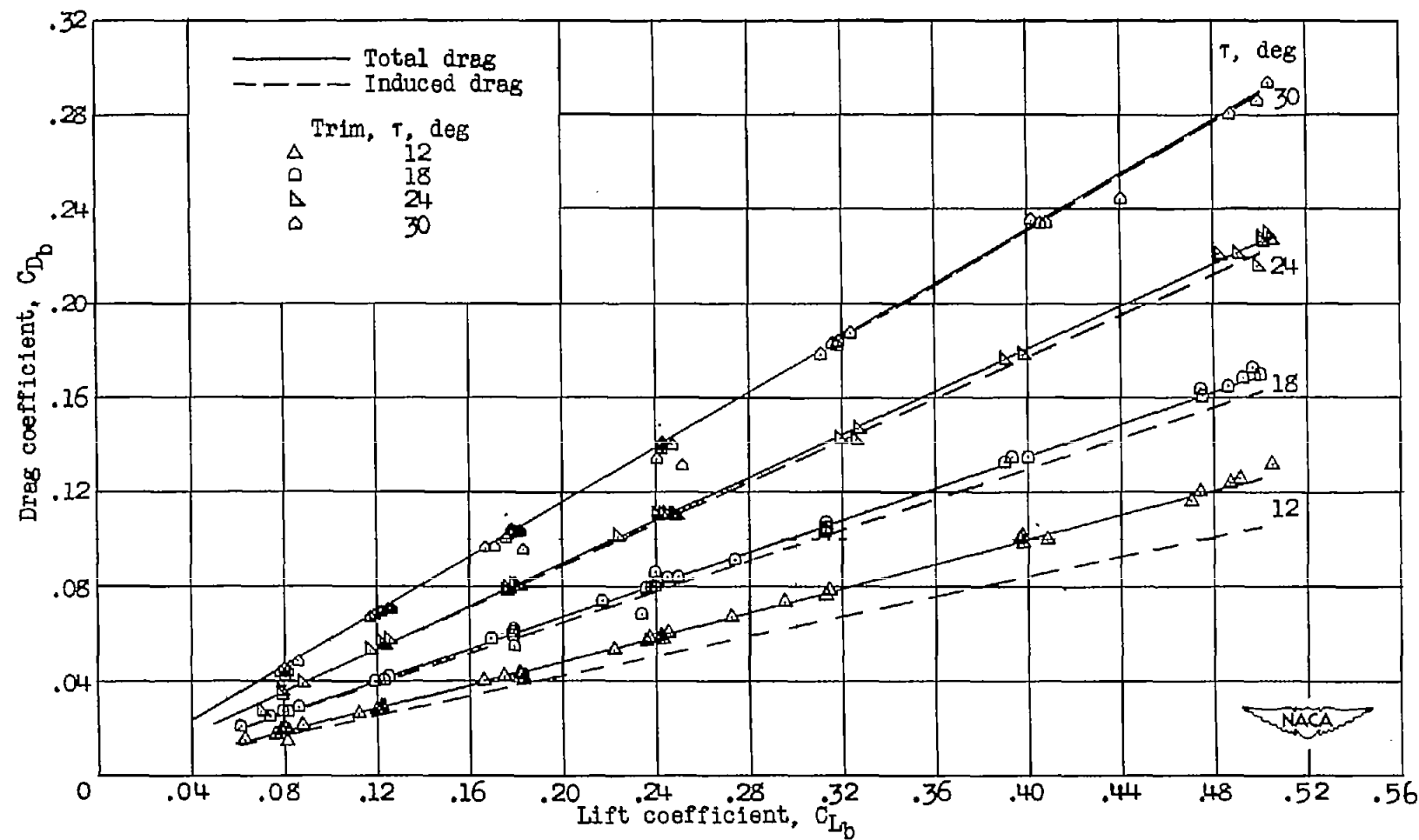
(b) Trim,  $12^\circ$ ,  $18^\circ$ ,  $24^\circ$ , and  $30^\circ$ .

Figure 18.- Concluded.

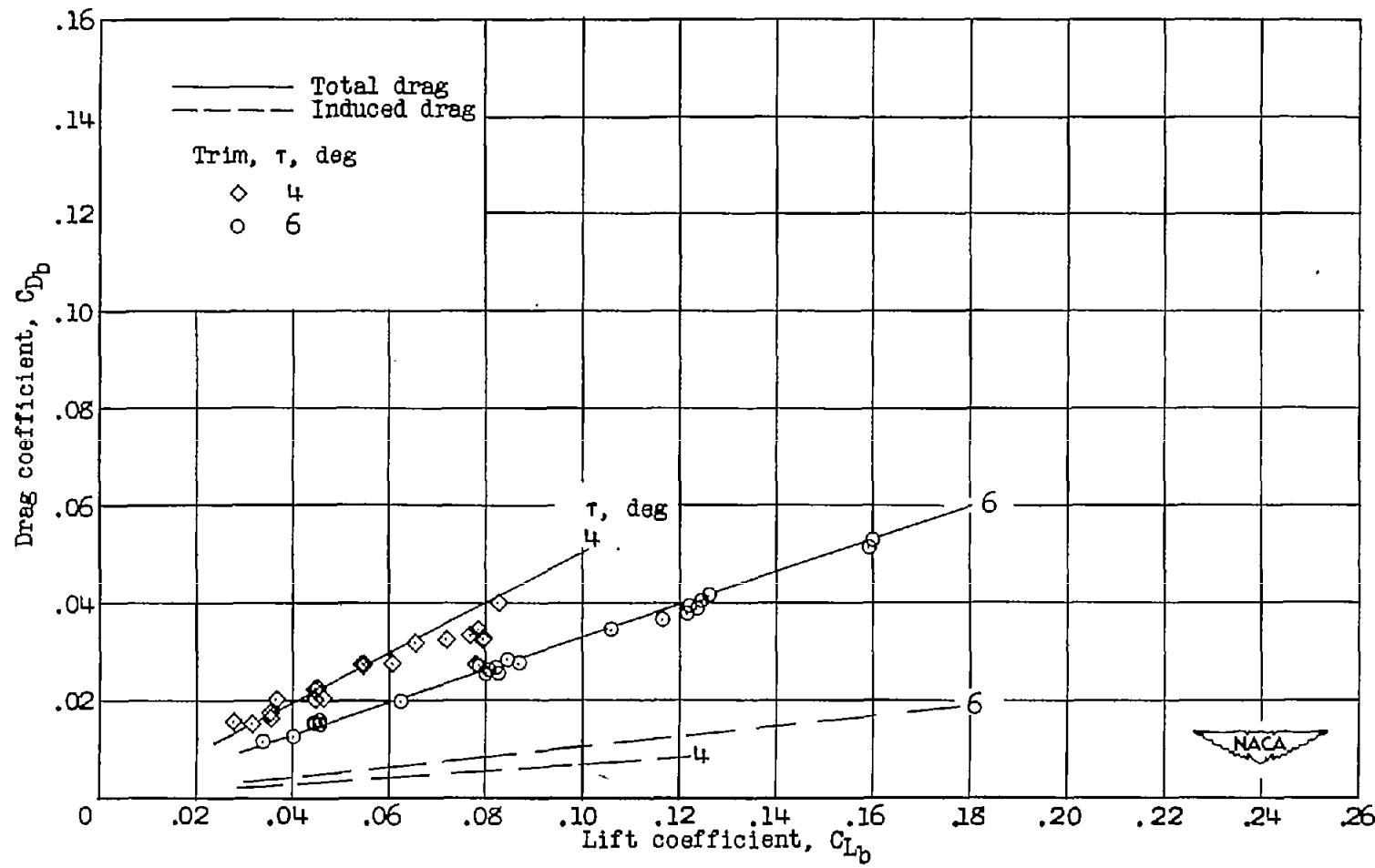
(a) Trim,  $4^\circ$  and  $6^\circ$ .

Figure 19.- Variation of drag coefficient with lift coefficient for surface having a  $40^\circ$  angle of dead rise.

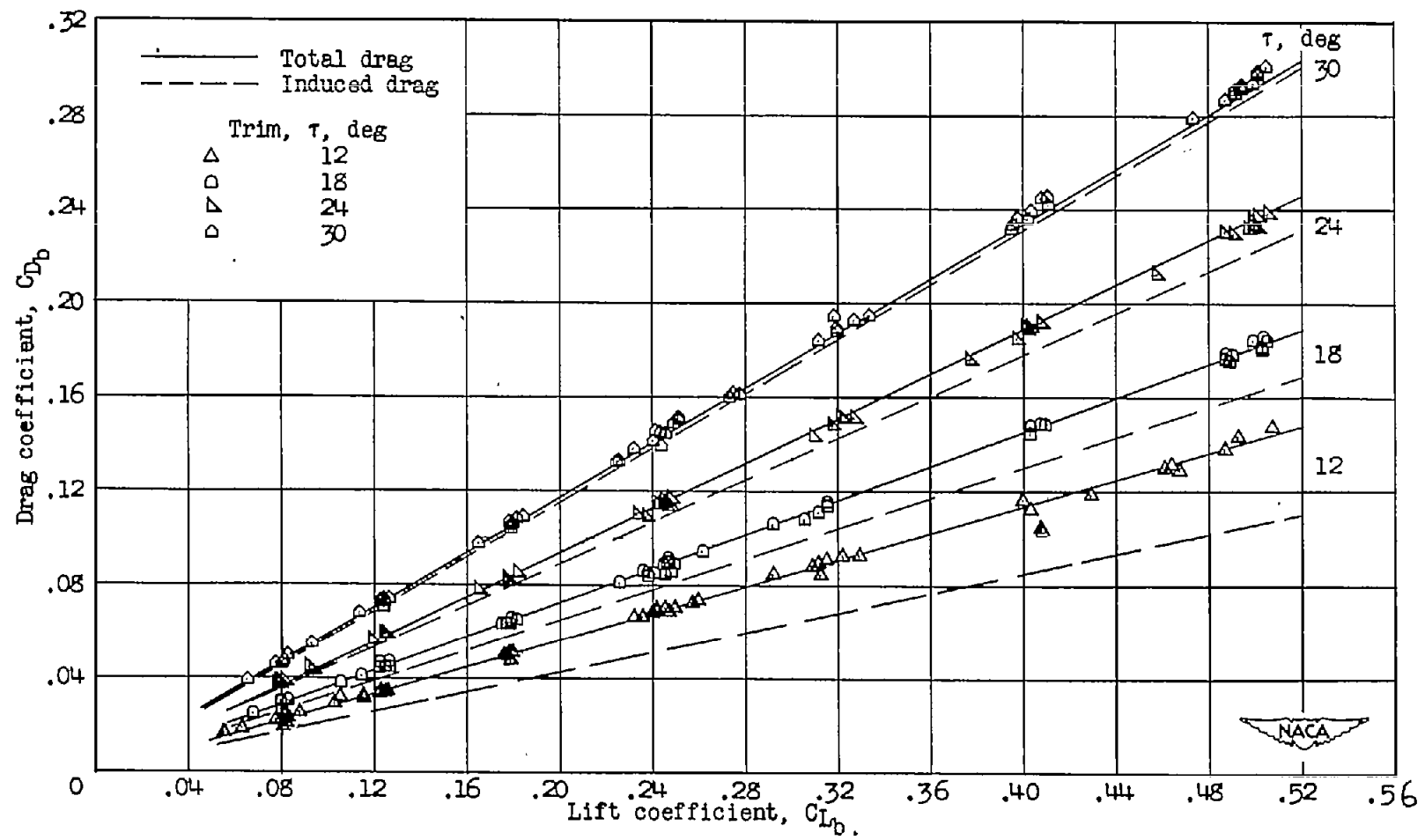
(b) Trim,  $12^\circ$ ,  $18^\circ$ ,  $24^\circ$ , and  $30^\circ$ .

Figure 19.- Concluded.

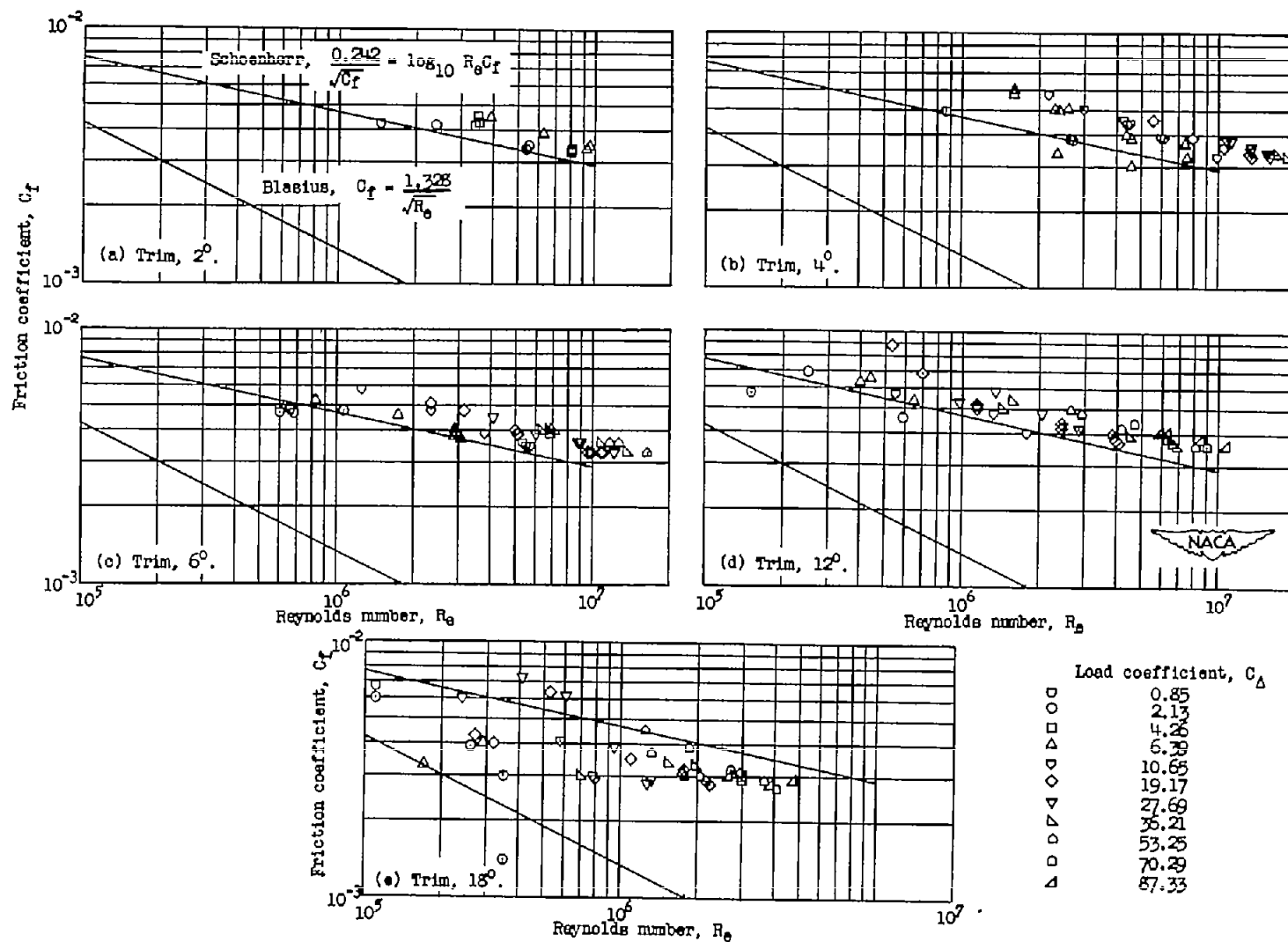


Figure 20.- Variation of friction coefficient with Reynolds number for surface having a  $20^\circ$  angle of dead rise.

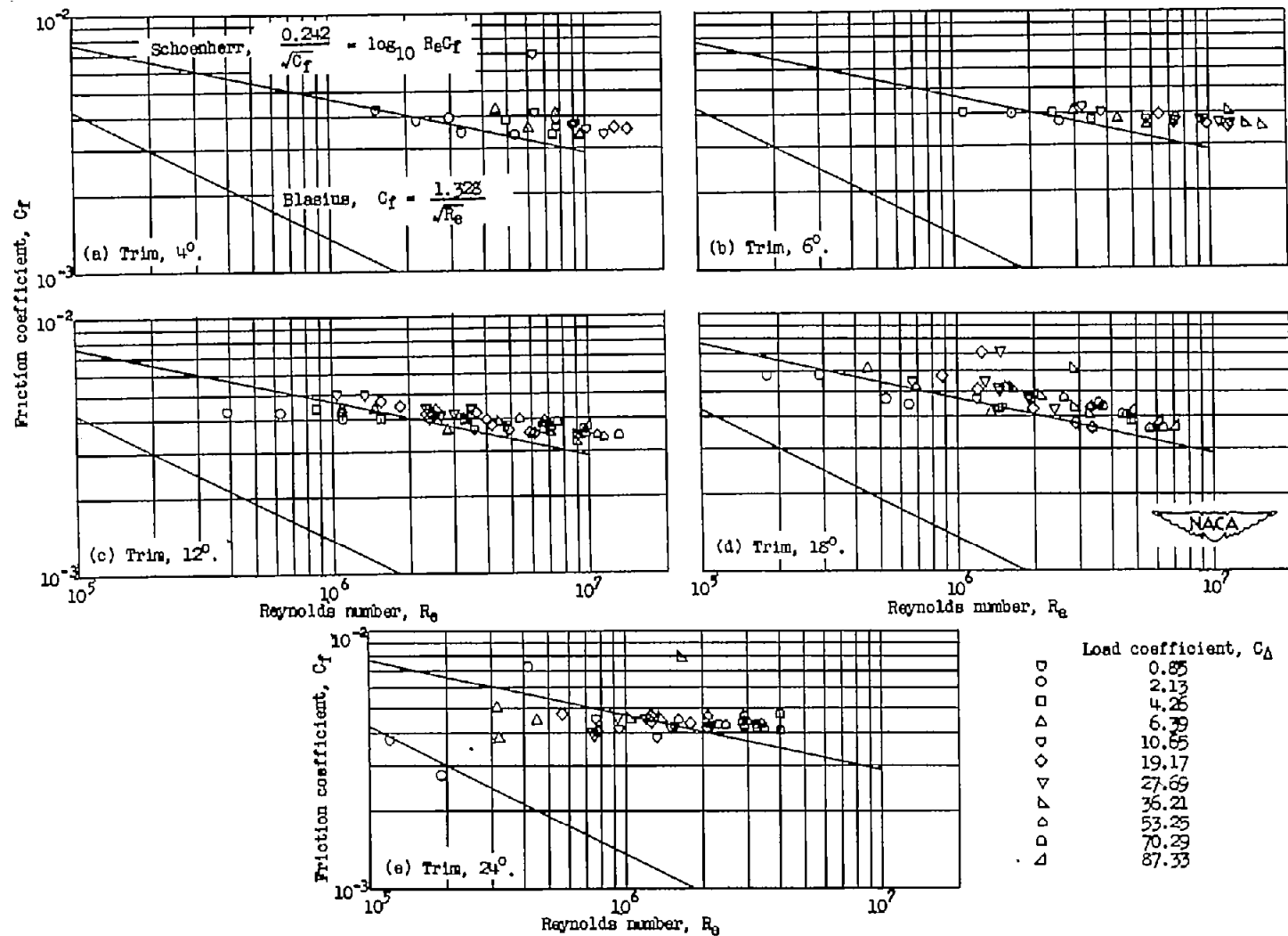


Figure 21.- Variation of friction coefficient with Reynolds number for surface having a  $40^{\circ}$  angle of dead rise.